Pivotal role of carrier scattering for semiconductorlike transport in math xmlns="http://www.w3.org/1998/Math/MathML">mrow>msub>mi>Fe/mi>mn>2/mn>/msub>mi>VAl/mi>/mrow>/math>

Fabian Garmroudi, Michael Parzer, Alexander Riss, Andrej Pustogow, Takao Mori, and Ernst Bauer

Phys. Rev. B **107**, L081108 — Published 16 February 2023

DOI: 10.1103/PhysRevB.107.L081108

Pivotal role of carrier scattering for semiconductorlike transport in Fe_2VAl

Fabian Garmroudi,[1,*] Michael Parzer,[1] Alexander Riss,[1] Andrej Pustogow,[1] Takao Mori,[2,3] and Ernst Bauer[1]

[1] *Institute of Solid State Physics, TU Wien, A-1040 Vienna, Austria*
[2] *International Center for Materials Nanoarchitectonics (WPI-MANA), National Institute for Materials Science, Tsukuba 305-0044, Japan*
[3] *University of Tsukuba, Tsukuba 305-8577, Japan*

A quarter century ago, a semiconductorlike resistivity was observed in the ternary Fe_2VAl Heusler alloy, sparking great interest in this material. Here, we reinvestigate the origin of this temperature-dependent behavior by simultaneously analyzing experimental resistivity, Seebeck and Hall effect data in the framework of a two-band model with different energy-dependent electron relaxation times. We reveal the pivotal role of an anomalous carrier scattering mechanism off localized antisite defect states in a nominally stoichiometric and seemingly well-ordered sample, which is crucial for comprehending the semiconductorlike transport. Our work demonstrates the benefit of concurrently probing complementary transport properties such as Seebeck coefficient, Hall mobility and electrical resistivity for understanding electronic transport phenomena in complex materials.

The electrical resistivity ρ is a fundamental property of materials related to electronic charge transport. It has been a long-standing challenge of condensed-matter physics to describe why certain materials are metals while others are insulators. The temperature dependence of $\rho(T)$ results from the changes of carrier concentration n, effective mass m and scattering rate τ^{-1} with energy and temperature. Yet, disentangling these separate contributions to the resistivity remains an unsolved puzzle for many complex systems, such as bad and strange metals [1–3] or unconventional superconductors [4]. Temperature-dependent charge transport in metals is dominated by carrier scattering, commonly yielding $d\rho/dT > 0$, while thermal activation across an energy gap results in a non-metallic slope $d\rho/dT < 0$ in insulators and semiconductors. Here, we identify scattering-dominated transport up to room temperature in Fe_2VAl, despite $d\rho/dT < 0$ in this range.

In 1997, Nishino *et al.* reported a semiconductorlike behavior of resistivity for the ternary Heusler alloy Fe_2VAl, in spite of metallic photoemission spectra [5], launching a wave of studies on this material [6–11]. A few years later, investigating the frequency- and temperature-dependent optical conductivity, Okamura *et al.* observed a pseudogap near the Fermi level and argued that these observations fully explain the semiconductorlike resistivity of Fe_2VAl [12]. Recent studies have suggested that an almost zero or small positive band gap describes the transport properties, especially the Seebeck coefficient, most accurately [13–15]. However, all previous studies that have attempted to comprehend the electronic transport based on phenomenological band models or *ab initio* calculations have considered either a constant relaxation time or dominant acoustic phonon scattering with weak energy dependence $\tau^{-1} \propto \sqrt{E}$ (see Fig. 1). While these are valid assumptions for most materials, here we emphasize that even in nominally stoichiometric Fe_2VAl intrinsic antisite defects cause severe modifications of the electronic scattering rate as a function of energy and temperature, which has been neglected so far. In a rigorous step-by-step approach we simultaneously assess the Seebeck coefficient $S(T)$, resistivity $\rho(T)$ and Hall effect of this complex material in a broad range of temperatures.

High-quality polycrystalline samples were synthesized by induction melting with negligible mass loss $\approx 0.05\,\%$. Low-temperature ($4-300\,\mathrm{K}$) experimental data of Seebeck coefficient and resistivity were obtained from our in-house setups. The resistivity was measured with an a.c. resistance bridge using the four-probe method. The

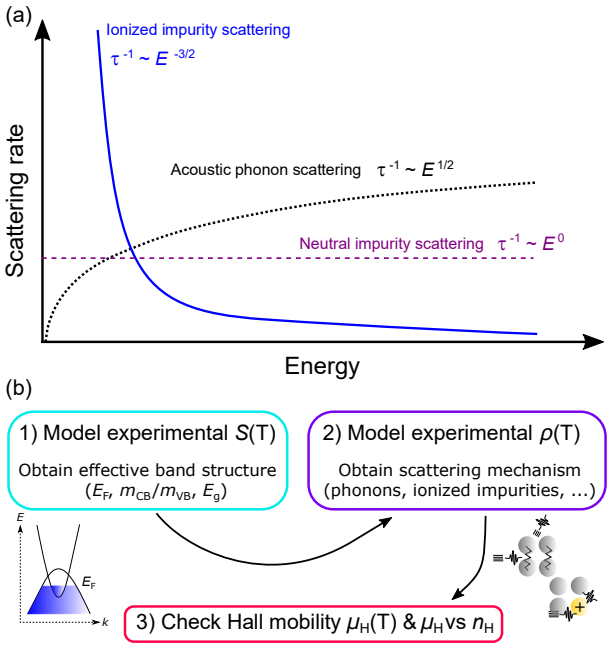

FIG. 1. (a) Sketch of electronic scattering rate as a function of energy for different scattering processes. (b) Schematic of our step-by-step approach to correctly model the electronic transport properties of the Fe_2VAl compound.

* fabian.garmroudi@tuwien.ac.at

Seebeck coefficient was measured with a toggled heating technique using chromel-constantan thermocouples. The Hall mobility was obtained by extracting the linear field dependence from the Hall resistivity measured with a PPMS by Quantum design from 0 to 9 T. A sample rotator was used to cancel spurious voltage contributions. Thermoelectric measurements from 300 to 800 K were performed by making use of a commercial setup (ULVAC-ZEM3). Seebeck and resistivity data were taken from our previous study where the sample quality (residual resistivity, maximum Seebeck coefficient) was especially high [16]. Additionally, samples with composition $Fe_2VAl_{1-x}Si_x$ (x = 0.025, 0.05, 0.075, 0.1) were newly synthesized for the investigation of the Hall mobility.

Previous optical spectroscopic studies on correlated electron systems at the edge of a Fermi-liquid instability succeeded in disentangling the temperature dependence of intrinsic parameters like the effective mass and scattering rate via the extended Drude model [17, 18]. Here, we take another route based on a synergistic combination of complementary transport measurements on the same sample: In order to simultaneously model the temperature-dependent electronic transport properties, we calculated $S(T)$ and $\rho(T)$ in the Fermi integral formalism within semiclassical Boltzmann transport theory:

$$S(T) = \frac{k_B}{e}\left[\frac{(\lambda+2)F_{1+\lambda}}{(\lambda+1)F_\lambda} - \eta\right], \quad \rho(T) = \mathcal{A}\frac{m}{F_\lambda}. \qquad (1)$$

Here, F_i are the Fermi integrals of ith order, $\eta = \mu/k_B$ is the reduced chemical potential and λ is a scattering parameter, which determines the energy dependence of the electronic scattering rate $\tau^{-1} \propto E^{1/2-\lambda}$; $\mathcal{A}$ is a constant prefactor. For the dominant scattering off acoustic phonons $\lambda = 0$, whereas $\lambda = \frac{1}{2}$ for neutral impurity scattering and $\lambda = 2$ is usually considered for ionized impurity scattering [19]. Note that only the latter case leads to a scattering rate which decreases with energy, signaling that low-energy carriers get scattered more strongly as they get trapped in the Coulomb potential of ionized impurities. Additionally to the energy-dependent term, τ^{-1} is proportional to a temperature-dependent term, which is $\sim T^2$ in Fermi liquids, $\sim T^{3/2}$ for dominant acoustic phonon scattering and $\sim T^{-3/2}$ for ionized impurity scattering [20, 21]. Since this term cancels out in the transport equations of $S(T)$ and becomes only relevant for $\rho(T)$, we started our analysis by modelling $S(T)$ to obtain information on the band structure/density of states (band gap, effective masses, chemical potential). We then proceeded to model $\rho(T)$ using the exact same band parameters to obtain information on the relevant scattering mechanism (see Fig. 1(b)). During this step, only a single parameter, the constant prefactor $\mathcal{A}$, needs to be fitted, since the energy and temperature dependence for the dominant scattering mechanism are fixed *a priori*. Therefore, this two-step analysis ensures unambiguous results with minimal number of free parameters.

Fig. 2 shows $S(T)$ and $\rho(T)$ of Fe_2VAl in a broad temperature range from 4 to 800 K. The distinct maximum of $S(T)$ directly correlates to the size of the (pseudo) band gap [14, 15] and the semiconductorlike behavior of $\rho(T)$ is in good agreement with previous studies [5]. Solid and dashed lines are model results for different values of λ. While the experimental Seebeck coefficient can be accurately described by both models, the fitted band gap varies dramatically depending on the value of λ (see inset Fig. 2(a)). More importantly, it can be seen that acoustic phonon scattering completely fails at describing the qualitative nature of the resistivity, resulting in metallic behavior, $d\rho/dT > 0$, at low temperatures. In other words, the increase of the carrier concentration $n(T)$ due to charge carriers getting excited across the (pseudo) gap becomes overshadowed and outweighed by the rapid increase of carrier scattering with increasing temperature. The same qualitative scenario holds true for any scattering rate which increases with increasing temperature.

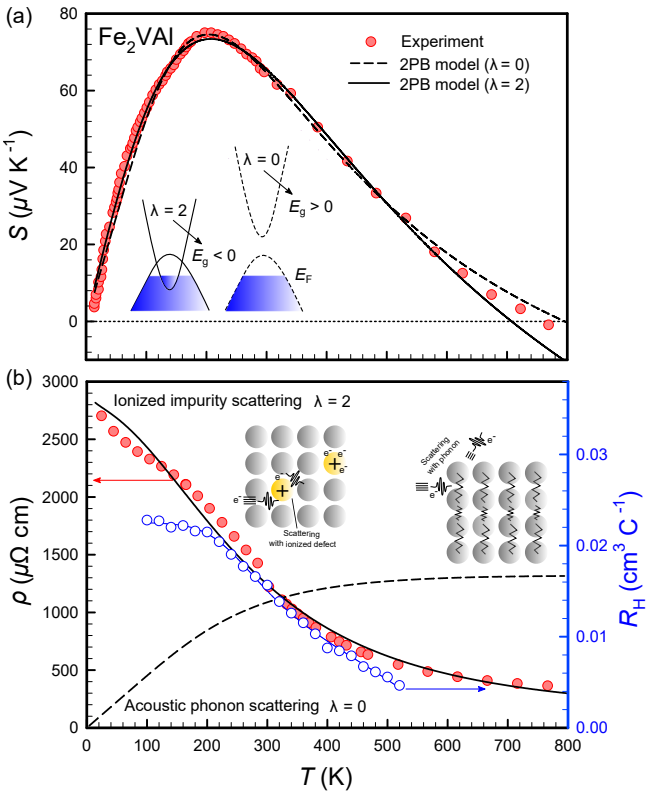

FIG. 2. Temperature-dependent Seebeck coefficient (a) and electrical resistivity (b) of Fe_2VAl. Open symbols in (b) correspond to the measured Hall coefficient, which tends towards saturation around 200 K. Dashed and solid lines are least-squares fits, obtained from a parabolic two-band model with different scattering mechanisms. Insets sketch the band structures and scattering processes. The scattering parameter λ for the transport model is chosen *a priori*, which gives different band gaps from the Seebeck modelling. In a second step, the choice of the correct scattering process and λ can be verified by modelling the resistivity using the same band parameters obtained from the previous step.

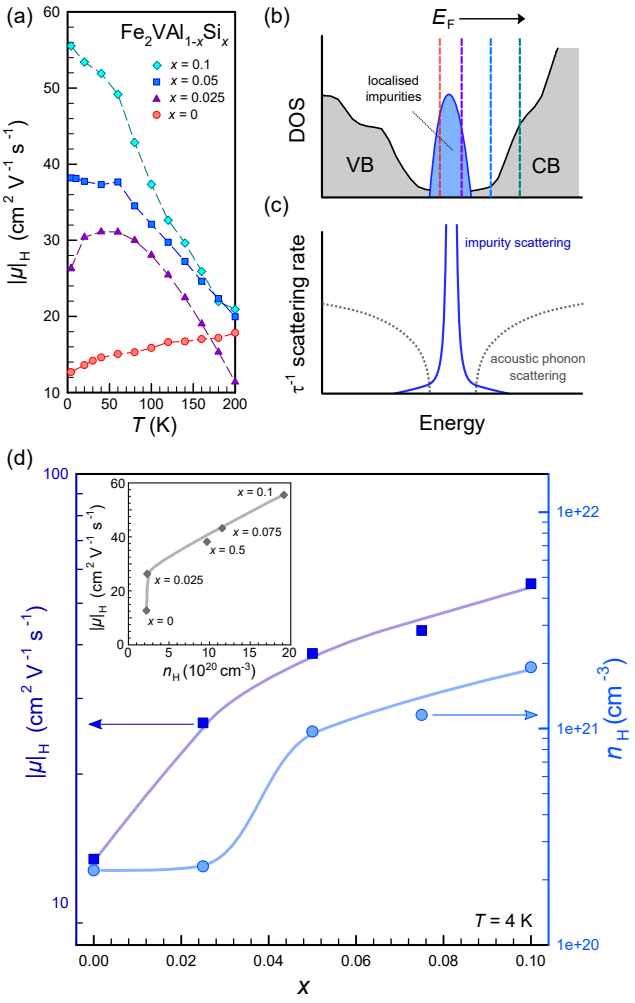

FIG. 3. (a) Temperature-dependent Hall mobility of $Fe_2VAl_{1-x}Si_x$ full-Heusler compounds. (b) Sketch of density of states and (c) energy-dependent scattering rate of $Fe_2VAl_{1-x}Si_x$ in the presence of small amounts of antisite disorder. (d) Hall mobility and carrier concentration as a function of Si concentration. Inset shows the residual Hall mobility versus the residual carrier concentration. Solid lines are guides to the eye.

On the other hand, only when considering an anomalous scattering rate which decreases with energy and temperature, e.g. $\tau^{-1} \sim T^{-3/2}E^{-3/2}$, both $S(T)$ and $\rho(T)$ can be simultaneously described by the same band structure parameters. Moreover, when analyzing the Hall coefficient R_H (open symbols in Fig. 2(b)), it can be seen that R_H tends towards saturation below room temperature, implying that the carrier concentration does not vary much in this temperature range. Thus, the carrier mobility determines the semiconductorlike resistivity behavior below room temperature.

We argue that small amounts of intrinsic antisite defects, which naturally occur upon synthesis and/or heat treatment [22, 23], trap and temporarily localize charge carriers. More specifically, Fe_V, V_{Fe} and Fe_{Al} antisite defects lead to in-gap impurity states, as evident from density functional theory (DFT) calculations [23–25]. A higher density of defects leads to a doping-like effect, which brings about a reduction of residual resistivity ρ_0 and maximum Seebeck coefficient S_{max}. Both, ρ_0 and S_{max} of the data discussed in this work, are comparable or higher compared to the as-cast and furnace-cooled samples discussed in our recent study [23]. It should be noted that below a critical concentration of defects, these impurity states, are localized due to Anderson and Mott localization, and therefore do not substantially contribute to $S(T)$ and $\rho(T)$ via band-like transport themselves. Nevertheless, we stress that strong modifications of the temperature- and energy-dependent scattering of conduction electrons can occur when the Fermi level is placed in the vicinity of these defect states. Moreover, recent DFT calculations showed that there occurs a significant charge transfer from Al towards Fe and V atoms in the Fe_2VAl compound [14].

However, the situation is completely different for the antisite atoms, resulting in different ionicities of the main lattice and the antisite defects. Indeed, an anomalous behavior of the temperature-dependent Hall mobility is found for Fe_2VAl, both as a function of temperature and when varying the position of the chemical potential. Fig. 3(a) shows that $\mu_H(T)$ increases with temperature for undoped Fe_2VAl up to 300 K, which cannot be explained by conventional electron-phonon or electron-electron scattering as these mechanisms involve an increase of scattering with rising temperature. However, doping excess carriers by substituting Si on the Al site in $Fe_2VAl_{1-x}Si_x$ gradually changes the temperature-dependence of $\mu_H(T)$ since E_F is shifted into the conduction band and the impurities become screened. For $x = 0.025$ a local maximum develops at around 50 K. The maximum vanishes when x is increased up to $x = 0.05$ until a monotonic decrease of $\mu_H(T)$ with temperature is observed for $x = 0.1$. Moreover, $|\mu|_H(T)$ increases despite the increase of the carrier concentration $n_H(T)$ and chemical disorder, hinting at a gradual change in the dominant scattering mechanism. As sketched in Fig. 3(b) the substitution of Al/Si shifts the chemical potential in a rigid-band-like manner, outside the localized in-gap states. This shift of E_F into the conduction band has also been confirmed experimentally (e.g. via measurements of the Seebeck coefficient) and theoretically in previous studies [15, 26–28]. Since the impurities become gradually screened, the impurity scattering off the antisite defects becomes consistently weaker until conventional scattering mechanisms dominate almost in the entire temperature range down to 4 K for $Fe_2VAl_{0.9}Si_{0.1}$. Fig. 3(c) shows that both the Hall carrier concentration and Hall mobility simultaneously increase with increasing carrier doping concentration x in $Fe_2VAl_{1-x}Si_x$. Such an anomalous behavior is at odds with what would be expected for conventional doping and hints at a gradual change in the dominant scattering mechanism as has been described above.

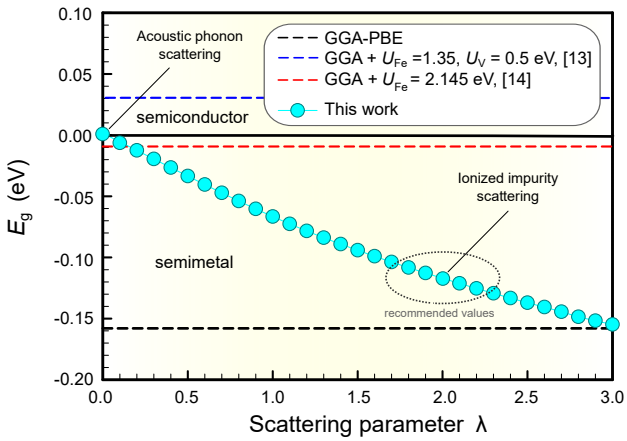

FIG. 4. Band gap of Fe_2VAl calculated for different scattering parameters λ. Our extensive analysis yields $\lambda \approx 2$ as the recommended value, hinting at a more negative energy gap than suggested in previous studies [13, 14].

Realizing the importance of using the appropriate scattering parameter when modelling the temperature-dependent transport properties of Fe_2VAl, we scanned a large range of λ values. Fig. 4 shows that the fitted energy gaps vary substantially due to the different energy dependences of τ^{-1}. $\lambda = 0$ yields a small positive band gap, which is only consistent with DFT calculations when including an on-site correction to the electronic correlation (GGA+U calculations) [13]. By increasing λ we obtain negative band gaps, which are closer to those predicted by simple GGA-PBE band-structure calculations. In other words, the carrier filtering due to intrinsic antisite defects near the Fermi energy brings about smaller values of the fitted pseudo band gap than one would expect when neglecting these essential effects on the electronic relaxation time. These results are also in stark contrast to the large positive band gaps (up to ~ 1 eV) obtained from DFT calculations employing hybrid functionals [24, 29] and manifest Fe_2VAl as a "bad semimetal" with $E_g \approx -0.11$ eV rather than a semiconductor with $E_g > 0$. The semiconductorlike transport thus arises to a great extent from the anomalous scattering and interplay of mobile charge carriers with localized defect states close to E_F. We note that when analyzing a different set of $S(T)$, $\rho(T)$ data from Ref. [11], we arrive at exactly the same conclusion regarding the pivotal role of carrier scattering as well as a similar negative band overlap ≈ -0.12 eV. Moreover, we applied the same two-band model to other prominent semimetallic and semiconducting members of the Heusler family. Table I shows the estimated band gaps of different Heusler-type compounds, for which transport data have been reported in a broad temperature range. For isovalent Fe_2VGa, similar conclusions regarding the importance of ionized impurity scattering can be made, which is not surprising since it was shown that Fe_2VGa is equally susceptible towards intrinsic antisite defects [30]. The value of $E_g \approx -0.23$ eV obtained from our analysis is in very good agreement with simple GGA band structure calculations ($E_g \approx -0.22$ eV) [31]. Very convincing predictions for E_g are also found in half-Heusler compounds. For instance, $E_g \approx 0.15$ eV is estimated for ZrNiSn, which is consistent with $E_g \approx 0.13$ eV obtained from optical diffuse reflectance measurements [32].

TABLE I. Band gaps of different Heusler-type compounds, obtained by modelling the temperature-dependent Seebeck coefficient assuming dominant acoustic phonon or ionized impurity scattering.

Material	E_g^{2PB} from Seebeck	Scattering parameter
Fe_2VAl [11]	-0.12 eV	$\lambda = 2$
Fe_2VAl [16]	-0.11 eV	$\lambda = 2$
Fe_2VGa [33]	-0.23 eV	$\lambda = 2$
TiNiSn [34]	0.67 eV	$\lambda = 0$
ZrNiSn [32]	0.15 eV	$\lambda = 0$
$ZrRu_{1.5}Sb$ [35]	0.44 eV	$\lambda = 0$
Ti_2FeSb_2 [36]	0.25 eV	$\lambda = 0$

In conclusion, we revisited the semiconductorlike transport behavior of Fe_2VAl and found that intrinsic defects and ionized atoms play a crucial role in understanding the temperature-dependent behavior even up to room temperature. Simultaneous experimental and theoretical investigation of the Seebeck coefficient, Hall effect and resistivity establish the importance of identifying the actual carrier scattering mechanism. Studying the Hall mobility of $Fe_2VAl_{1-x}Si_x$ with varying positions of the chemical potential reveals a gradual change in the dominant scattering mechanism from scattering off ionized impurity states towards electron-phonon scattering. Finally, bringing together all experimental observations, we demonstrate that Fe_2VAl is not a semiconductor but rather a "bad semimetal", with a pseudogap similar to that obtained by simple GGA-PBE calculations. Our work showcases that the pristine band structure is often insufficient to describe electronic transport properties of complex materials in the presence of disorder and defects, as they affect the electronic scattering rate. We suggest the combined analysis of complementary transport properties presented here as a powerful tool for unravelling the mysteries of bad metals and correlated electron systems.

Funding came from the Japan Science and Technology Agency (JST) program MIRAI, JPMJMI19A1.

[1] O. Gunnarsson, M. Calandra, and J. Han, Reviews of Modern Physics **75**, 1085 (2003).
[2] N. Hussey, K. Takenaka, and H. Takagi, Philosophical Magazine **84**, 2847 (2004).
[3] J. Bruin, H. Sakai, R. Perry, and A. Mackenzie, Science **339**, 804 (2013).
[4] B. Keimer, S. A. Kivelson, M. R. Norman, S. Uchida, and J. Zaanen, Nature **518**, 179 (2015).
[5] Y. Nishino, M. Kato, S. Asano, K. Soda, *et al.*, Physical Review Letters **79**, 1909 (1997).
[6] C.-S. Lue *et al.*, Physical Review B **58**, 9763 (1998).
[7] R. Weht and W. Pickett, Physical Review B **58**, 6855 (1998).
[8] D. Singh and I. Mazin, Physical Review B **57**, 14352 (1998).
[9] C.-S. Lue, J. H. Ross Jr, C. Chang, and H. Yang, Physical Review B **60**, R13941 (1999).
[10] Y. Feng, J. Rhee, T. Wiener, D. W. Lynch, B. Hubbard, A. Sievers, *et al.*, Physical Review B **63**, 165109 (2001).
[11] Y. Nishino, H. Kato, M. Kato, and U. Mizutani, Physical Review B **63**, 233303 (2001).
[12] H. Okamura, J. Kawahara, T. Nanba, S. Kimura, K. Soda, U. Mizutani, Y. Nishino, *et al.*, Physical Review Letters **84**, 3674 (2000).
[13] S. Anand, R. Gurunathan, T. Soldi, L. Borgsmiller, R. Orenstein, and G. J. Snyder, Journal of Materials Chemistry C **8**, 10174 (2020).
[14] B. Hinterleitner, F. Garmroudi, N. Reumann, T. Mori, E. Bauer, and R. Podloucky, Journal of Materials Chemistry C **9**, 2073 (2021).
[15] F. Garmroudi, A. Riss, M. Parzer, N. Reumann, H. Müller, E. Bauer, S. Khmelevskyi, R. Podloucky, T. Mori, *et al.*, Physical Review B **103**, 085202 (2021).
[16] I. Knapp, B. Budinska, D. Milosavljevic, P. Heinrich, S. Khmelevskyi, R. Moser, R. Podloucky, P. Prenninger, and E. Bauer, Physical Review B **96**, 045204 (2017).
[17] X. Deng, A. Sternbach, K. Haule, D. Basov, and G. Kotliar, Physical review letters **113**, 246404 (2014).
[18] A. Pustogow, Y. Saito, A. Löhle, M. Sanz Alonso, A. Kawamoto, V. Dobrosavljević, M. Dressel, and S. Fratini, Nature Communications **12**, 1 (2021).
[19] D. Young, T. Coutts, V. Kaydanov, A. Gilmore, Mulligan, and WP, Journal of Vacuum Science & Technology A: Vacuum, Surfaces, and Films **18**, 2978 (2000).
[20] E. Conwell and V. Weisskopf, Physical Review **77**, 388 (1950).
[21] D. Chattopadhyay and H. Queisser, Reviews of Modern Physics **53**, 745 (1981).
[22] S. Maier, S. Denis, S. Adam, J.-C. Crivello, J.-M. Joubert, and E. Alleno, Acta Materialia **121**, 126 (2016).
[23] F. Garmroudi, M. Parzer, A. Riss, A. V. Ruban, *et al.*, Nature Communications **13**, 1 (2022).
[24] D. I. Bilc and P. Ghosez, Physical Review B **83**, 205204 (2011).
[25] S. Bandaru and P. Jund, Physica Status Solidi (b) **254**, 1600441 (2017).
[26] Y. Nishino, S. Deguchi, and U. Mizutani, Physical Review B **74**, 115115 (2006).
[27] C. S. Lue, C. Chen, J. Lin, Y. Yu, and Y. Kuo, Physical Review B **75**, 064204 (2007).
[28] F. Garmroudi, M. Parzer, A. Riss, S. Beyer, S. Khmelevskyi, T. Mori, M. Reticcioli, and E. Bauer, Materials Today Physics **27**, 100742 (2022).
[29] S. S. Shastri and S. K. Pandey, Computational Materials Science **143**, 316 (2018).
[30] C.-S. Lue, J. H. Ross Jr, K. Rathnayaka, D. Naugle, S. Wu, and W. Li, Journal of Physics: Condensed Matter **13**, 1585 (2001).
[31] M. Khalfa, H. Khachai, F. Chiker, N. Baki, K. Bougherara, A. Yakoubi, G. Murtaza, M. Harmel, M. Abu-Jafar, S. B. Omran, *et al.*, International Journal of Modern Physics B **29**, 1550229 (2015).
[32] J. Schmitt, Z. M. Gibbs, G. J. Snyder, and C. Felser, Materials Horizons **2**, 68 (2015).
[33] P.-C. Wei, T.-S. Huang, S.-W. Lin, G.-Y. Guo, and Y.-Y. Chen, Journal of Applied Physics **118**, 165102 (2015).
[34] S.-W. Kim, Y. Kimura, and Y. Mishima, Intermetallics **15**, 349 (2007).
[35] L. Wang, Z. Dong, S. Tan, J. Zhang, W. Zhang, and J. Luo, Advanced Functional Materials , 2200438 (2022).
[36] R. Hasan, T. Park, S.-i. Kim, H.-S. Kim, S. Jo, and K. H. Lee, Advanced Energy and Sustainability Research **3**, 2100206 (2022).